Experimental creep behaviour determination of cladding tube materials under multi-axial loadings

Catherine Grosjean [a,b,*], Dominique Poquillon [b], Jean-Claude Salabura [b], Jean-Marc Cloué [a]

[a] *AREVA, Areva NP, Fuel Business Unit, Lyon, France*
[b] *Université de Toulouse; CIRIMAT; Toulouse, France*

* Corresponding author. Tel.: +33 5 62 88 56 53; fax: +33 5 62 88 56 63.
E-mail address: catherine.grosjean@ensiacet.fr (C. Grosjean).

A B S T R A C T

Cladding tubes are structural parts of nuclear plants, submitted to complex thermomechanical loadings. Thus, it is necessary to know and predict their behaviour to preserve their integrity and to enhance their lifetime. Therefore, a new experimental device has been developed to control the load path under multi-axial load conditions. The apparatus is designed to determine the thermomechanical behaviour of zirconium alloys used for cladding tubes. First results are presented. Creep tests with different biaxial loadings were performed. Results are analysed in terms of thermal expansion and of creep strain. The anisotropy of the material is revealed and iso-creep strain curves are given.

Keywords:
Zirconium alloy
Anisotropy
Multi-axial loading
Thermal expansion
Creep strain

1. Introduction

The creep resistance of zirconium alloys is a major concern for the in-pile behaviour of fuel claddings used in fuel assemblies of pressurized water reactors (PWR and BWR). These fuel claddings – which constitute the first barrier against fuel leaks – are submitted to multi-axial creep loadings, mainly due to water pressure and to the production of gas during the nuclear reactions in the fuel pellets [1]. That is why these structural elements have been largely investigated for years [2–4]. Nevertheless, few data are available on multi-axial loading, especially during the creep tests. Furthermore, the influence of the loading path on the behaviour of fuel claddings remains unexplored, even if this parameter can have a strong influence in the case of anisotropic materials. Therefore a new device has been developed to control the load path during creep test, to enlarge the data base required to study its impact on creep behaviour. In the first part of the paper, the device and the material tested are presented. Then experimental results will be given and discussed.

2. Materials and experimental procedure

2.1. Materials

The investigated zirconium alloy in this study is a stress-relieved Zircaloy 4, which has already been previously investigated [5–7]. The interest in such an alloy is the possibility to compare the previous and present results on its mechanical behaviour to validate the newly developed experimental device. Its chemical composition is given in Table 1.

The specimens used are segments of fuel claddings. These tubes present an outer diameter of 9.51 mm, and an inner diameter of 8.35 mm (cf. Fig. 1). They have been formed by a cold pilgering process, which induces a noticeable and characteristic crystallographic texture [8]. Thus, the zirconium alloys which are already intrinsically anisotropic due to their hexagonal compact structure, have its anisotropy enhanced by the forming process [9]. This anisotropy influences the mechanical behaviour of the tested fuel claddings.

2.2. Experimental setup

The experimental setup has been developed to control the thermomechanical loadings of cladding tube specimen. This apparatus can be divided into independent subsystems as detailed in Fig. 2.

Firstly, the specimen is constituted of a 130 mm long tube and its clamping set [10] (Fig. 1). On this tube, two alloy 718 strips are spot-welded to delimit the gauge length (20 mm centred on the middle of the tube), and used to follow the axial deformations. Three thermocouples are also spot-welded on the sample to control and regulate the temperature of the three zones radiative furnace.

Two couples of laser transmitter/receptor are used to follow the change of the gauge length z and of the outer diameter of the tube, $2r_{ext}$. The axial and the hoop strain are deduced from these measurements.

Table 1
Chemical composition of Zircaloy 4 alloys (wt.%, ASTM Standard).

Sn	1.20–1.70
O	0.10–0.14
Fe	0.18–0.24
Cr	0.07–0.13
Zr	Bal.

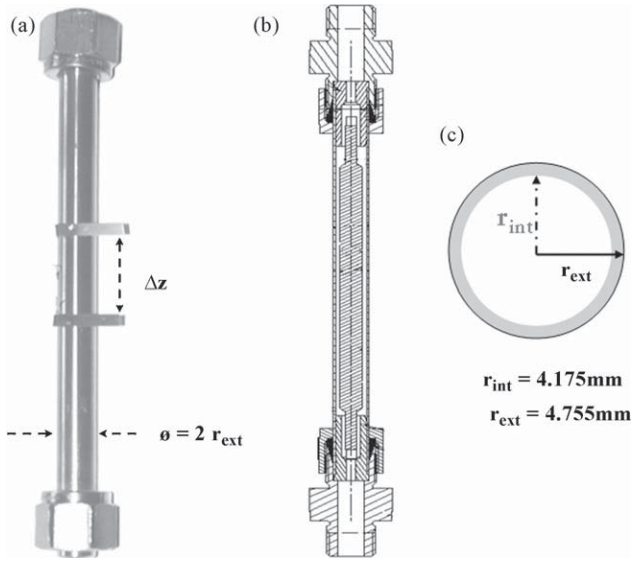

Fig. 1. Specimen set up, face (a), (b) and top (c) figures.

$$\varepsilon_{zz} = \ln\left(1 + \frac{z - z_0}{z_0}\right) \qquad \varepsilon_{\theta\theta} = \ln\left(1 + \frac{\phi - \phi_0}{\phi_0}\right)$$

The apparatus uses a tensile and compression electromechanical device to submit the sample to an axial load which enables loadings up to 10 kN with an accuracy of ±2 N. The pressurizing and regulating system can load the sample to hoop stress $\sigma_{\theta\theta}$ up to 150 MPa (±0.5 MPa).

The distinctive feature of this device is the simultaneous use of a radiative furnace, laser extensometers, an open pressuring system and a tensile and compression electromechanical device. Indeed, radiative furnace have already been used by Kaddour [11,12]. Laser extensometers have been used by Ferrer or Onimus [13,14]. In Ref. [12], Earthman and Murty studied the creep of Zycraloy-4 with specimens made of open tubes pressurized by an inert gas to submit the sample to a hoop stress controlled by the pressure level. But as they used static load to impose the axial load to the sample, they were not able to control precisely the load path.

By the way, the present apparatus allows us to control the axial and hoop stresses. Furthermore, the temperature difference on the 20 mm gauge length is less than 0.5 K and both axial and hoop strains versus time are collected.

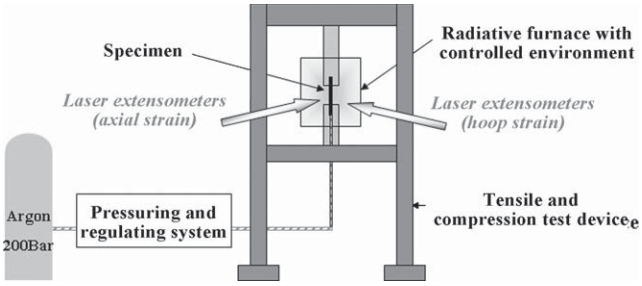

Fig. 2. Scheme of the new device.

2.3. Experimental procedure

The purpose of the tests carried out on this new device is to control the temperature, the hoop and the axial stress during the whole thermo-mechanical loading. For the tests detailed in the present study, the experimental procedure depends on the biaxiality ratio β of the creep test, which is the ratio of the axial stress σ_{zz} to the hoop stress $\sigma_{\theta\theta}$.

$$\beta = \frac{\sigma_{zz}}{\sigma_{\theta\theta}}$$

If S is the cross-section of the tube, P the imposed pressure inside the tube, F the axial load, r_{ext} the outer radius of the cladding tube and r_{int} its inner radius (cf. Fig. 1), then the following relations can be used for this thin tube geometry, in which the radial stress σ_{rr} can be neglected [15]:

$$\sigma_{zz} = \frac{F}{S} + \frac{P}{4}\frac{(r_{ext} + r_{int})}{(r_{ext} - r_{int})} \text{ and } \sigma_{\theta\theta} = \frac{P}{2}\frac{(r_{ext} + r_{int})}{(r_{ext} - r_{int})}$$

When pressure is needed to reach a given value of the hoop stress ($\sigma_{\theta\theta}$), the air tightness is checked before positioning the furnace. Then, all the tests follow the same procedure. A small axial load corresponding to 3 MPa is applied to the tube in order to avoid buckling during thermal loading. The heating is then imposed from room temperature to 673 K (400 °C) at 50 K/min. The temperature stabilization in the whole device is reached after 15 min. Then the imposed mechanical loading is monitored and data from the extensometers and the load cell are collected at a frequency of 1 Hz. The strain rate during loading was set to 10^{-6} s^{-1} except for tests 1 and 2 [10^{-3} s^{-1}] and tests 3 and 4 [10^{-4} s^{-1}].

The purpose of the creep tests carried out in the present work is to study the strain rates during the steady state. So tests are stopped when secondary creep is stabilized and before reaching the tertiary creep.

3. Results

The first tests were done to validate results obtained with the new device. Thus, 14 creep tests have been carried out with different biaxiality ratio β [from 0.25 to ∞]. The purpose was (i) to check the results obtained on that device compared to previous experimental data, (ii) to validate the range of biaxiality that could be controlled and maintained during creep tests on the new device and (iii) to get first creep strain results to help to determine further testing programs.

The first step in the data analysis is the determination of the axial and hoop strains, and their representation versus time (cf. Fig. 3). From this one, important information will be deduced such as the axial and hoop coefficients of thermal expansion, and the steady-state creep strain rates.

Table 2 summarized the results concerning the thermal behaviour obtained during these tests. Indeed, the anisotropy of dilatation of the material is evidenced during heating. The average value of the coefficient of thermal expansion is 5.1×10^{-6} K^{-1} in the axial direction (α_{zz}) and 8.3×10^{-6} K^{-1} in the circumferential direction ($\alpha_{\theta\theta}$). As a consequence, the average ratio between these thermal expansion coefficients is close to 0.6.

Table 3 summarizes all the creep results. Tests labelled from 1 to 14 were carried out during the first campaign devoted to test the device. For each creep test, the ratio r of the axial strain rate $\dot{\varepsilon}_{zz}$ over the hoop strain rate $\dot{\varepsilon}_{\theta\theta}$ is determined.

$$r = \frac{\dot{\varepsilon}_{zz}}{\dot{\varepsilon}_{\theta\theta}}$$

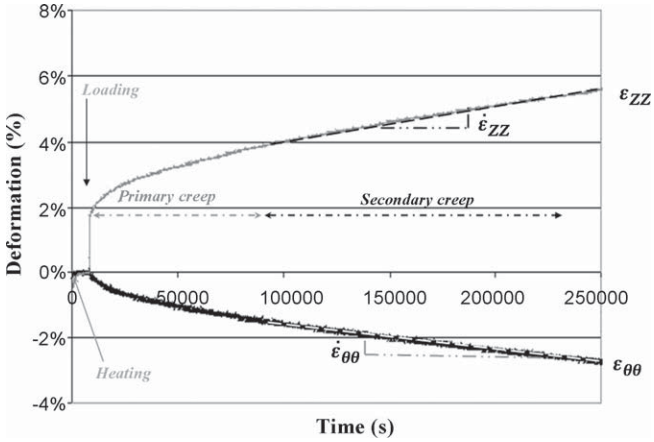

Fig. 3. Example of experimental data showing the axial and hoop strains versus time for an uniaxial creep test under 135 MPa, at 623 K.

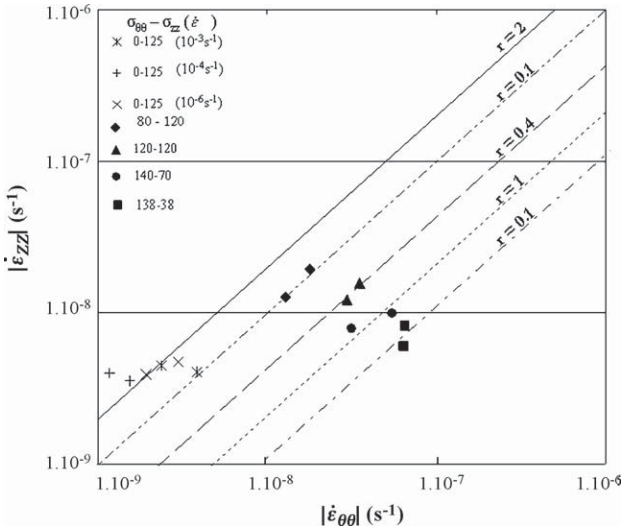

Fig. 4. Plot of the stationary axial and hoop creep strain rates.

Table 2
Hoop and axial coefficients of thermal expansion obtained on stress-relieved Zircaloy 4.

Test label	$\sigma_{\theta\theta}$ [MPa]	σ_{zz} [MPa]	β	$\dot{\varepsilon}$ [s^{-1}]	20–400 °C	
					$\alpha_{\theta\theta}$ [10^{-6} K^{-1}]	α_{zz} [10^{-6} K^{-1}]
1	0	125	∞	10^{-3}	8.97	5.13
2	0	125	∞	10^{-3}	8.06	4.79
3	0	125	∞	10^{-4}	7.58	5.53
4	0	125	∞	10^{-4}	9.14	5.67
5	0	125	∞	10^{-6}	8.73	5.62
6	0	125	∞	10^{-6}	6.77	5.13
8	80	120	1.5	10^{-6}	7.67	5.58
9	120	120	1	10^{-6}	8.17	3.94
11	140	70	0.5	10^{-6}	8.55	5.43
12	140	70	0.5	10^{-6}	7.50	4.19
13	138	38	0.25	10^{-6}	6.87	5.03

In the case of a uniaxial creep test, biaxiality ratio β is infinite. For isotropic material then $r = -2$ [15]. Data obtained during the experiments are not far from this value (see Table 3). Different strain rates have been used during loadings for the tests labelled 1 to 6 in order to see if the initial strain rate during loading influences the secondary creep strain rate. Between 10^{-6} s^{-1} and 10^{-3} s^{-1} no effect was observed (Table 3 and Fig. 4).

The creep tests carried out in multi-axial loading conditions enhanced the anisotropic behaviour of the tested materials (Fig. 2). For $\beta = 2$, $|r| \approx 1$; for $\beta = 1$, $|r| \approx 0.3$; for $\beta = 0.5$, $|r| \approx 0.2$ and $\beta = 0.25$, $|r| \approx 0.1$. A small value for the hoop strain rate strongly influences the r-value obtained and increases the uncertainty. However, the device allows carrying out all the tests planned. The results in terms of thermal behaviour, as well as in terms of mechanical behaviour are reproducible except for $\beta = 1$. Indeed, the value of r obtained for small stresses (cf. Table 3) differs from these obtained for larger stresses. New tests comparable to tests 19 and 20 should be done to check the values of r (cf. Table 2).

Table 3
Hoop and axial secondary creep strain rates obtained on stress-relieved Zircaloy 4 at 400 °C (σ^{VM} corresponds to Von Misès stress and $\dot{\varepsilon}$ to the equivalent creep strain rate).

Test label	β	$\sigma_{\theta\theta}$ (MPa)	σ_{zz} (MPa)	σ^{VM} (MPa)	Duration (h)	Secondary creep			
						$\dot{\varepsilon}_{\theta\theta}$ (s^{-1})	$\dot{\varepsilon}_{zz}$ (s^{-1})	$\dot{\varepsilon}$ (s^{-1})	r
1	∞	0	125	125	70	-1.53×10^{-9}	3.55×10^{-9}	3.76×10^{-9}	−2.32
2	∞	0	125	125	67	-1.16×10^{-9}	3.99×10^{-9}	4.10×10^{-9}	−3.44
3	∞	0	125	125	61	-2.37×10^{-9}	4.51×10^{-9}	4.91×10^{-9}	−1.90
4	∞	0	125	125	69	-3.86×10^{-9}	4.06×10^{-9}	5.14×10^{-9}	−1.06
5	∞	0	125	125	64	-2.99×10^{-9}	4.73×10^{-9}	5.32×10^{-9}	−1.58
6	∞	0	125	125	62	-1.92×10^{-9}	3.90×10^{-9}	4.20×10^{-9}	−2.03
7	1.5	80	120	106	18	1.28×10^{-8}	1.27×10^{-8}	1.64×10^{-8}	0.99
8	1.5	80	120	106	20	1.80×10^{-8}	1.94×10^{-8}	2.43×10^{-8}	1.08
9	1	120	120	120	21	3.52×10^{-8}	1.57×10^{-8}	3.27×10^{-8}	0.45
10	1	120	120	120	28	3.02×10^{-8}	1.28×10^{-8}	2.78×10^{-8}	0.42
11	0.5	140	70	121	22	5.47×10^{-8}	9.81×10^{-9}	4.57×10^{-8}	0.18
12	0.5	140	70	121	20	3.48×10^{-8}	7.89×10^{-9}	2.95×10^{-8}	0.23
13	0.25	138	38	123	29	6.46×10^{-8}	6.03×10^{-9}	5.31×10^{-8}	0.09
14	0.25	138	35	124	20	6.57×10^{-8}	8.11×10^{-9}	5.43×10^{-8}	0.12
15	∞	0	199	199	113	-5.87×10^{-9}	1.18×10^{-8}	1.27×10^{-8}	−2.01
16	∞	0	199	199	89	-7.39×10^{-9}	1.90×10^{-8}	1.99×10^{-8}	−2.57
17	2	56	112	97	65	3.31×10^{-9}	5.00×10^{-9}	5.68×10^{-9}	1.51
18	2	80	160	139	45	1.68×10^{-8}	1.84×10^{-8}	2.30×10^{-8}	1.10
19	1	76	76	76	88	7.87×10^{-9}	-2.89×10^{-9}	7.05×10^{-9}	−0.37
20	1	76	76	76	44	8.14×10^{-9}	-1.19×10^{-9}	6.75×10^{-9}	−0.15
21	0.5	84	42	73	67	8.72×10^{-9}	2.29×10^{-9}	7.48×10^{-9}	0.26
22	0.5	134	67	116	37	5.91×10^{-8}	1.47×10^{-8}	5.01×10^{-8}	0.25
23	0.5	110	55	95	48	2.35×10^{-8}	5.01×10^{-9}	1.98×10^{-8}	0.21

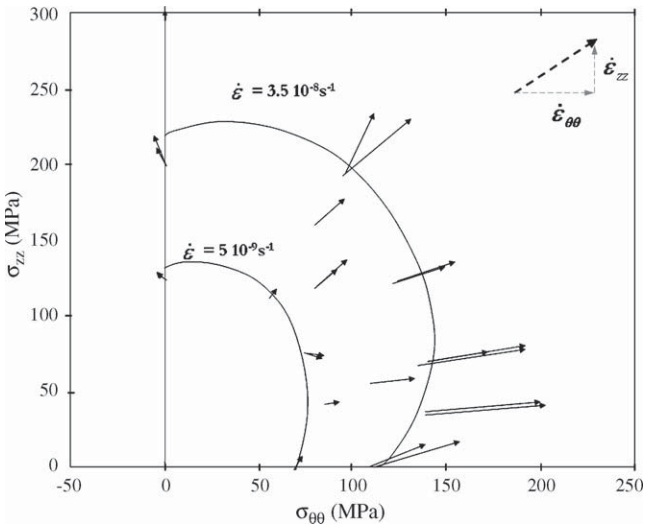

Fig. 5. Representation of the vectors of the creep strain rate (secondary creep) plotted for the different tested stress states. The arrows size is proportional to the creep strain rate.

In order to be able to plot iso-creep strain rate curves for different stress states, further creep tests were defined using a Norton creep law [16].

$$\dot{\varepsilon} = A\sigma^n$$

$$\text{with } \sigma = \sigma^{VM} = \frac{1}{\sqrt{2}} \times \sqrt{(\sigma_{rr}-\sigma_{\theta\theta})^2 + (\sigma_{\theta\theta}-\sigma_{zz})^2 + (\sigma_{zz}-\sigma_{rr})^2}$$

$$\text{and } \dot{\varepsilon} = \sqrt{\frac{2}{3} \times (\dot{\varepsilon}_{\theta\theta}^2 + \dot{\varepsilon}_{zz}^2)}$$

A value of $n = 4.3$ was identified after the first creep tests and additional tests were then defined to get results for a low strain rate of about $5 \times 10^{-9}\ s^{-1}$, and a medium strain rate of $3.5 \times 10^{-8}\ s^{-1}$. The purpose is to get iso-creep strain rate curves for these two strain rate levels. These curves correspond, for creep data, to the yield surfaces obtained for the plastic behaviour. However, plasticity mechanisms involved during slow strain rate creep tests can differ from those observed at higher strain rate.

Tests labelled from 15 to 22 given in Table 3 were obtained in this second creep tests campaign. The corresponding strain rates are closed to the awaited ones which were $5 \times 10^{-9}\ s^{-1}$ and $3.5 \times 10^{-8}\ s^{-1}$ (Table 3). The axial and hoop strains obtained for different stress states are plotted in Fig. 5 by the use of strain rate vectors, whose vertical and horizontal components are respectively $\dot{\varepsilon}_{zz}$ and $\dot{\varepsilon}_{\theta\theta}$. Thus the direction of the vector indicates the creep flow, and its position $\sigma_{\theta\theta}$ and σ_{zz} corresponds to the creep loading. From these results, we can interpolate the shape of the two iso-creep strain rate curves (dashed lines). Furthermore, for different biaxiality ratio, Norton coefficients can be calculated as shown in Fig. 6 and given in Table 4.

Table 4
Norton exponent as a function of the biaxiality ration for stress-relieved Zircaloy 4 at 400 °C.

β	n
∞	2.7
2	4.0
1	3.1
0.5	3.3

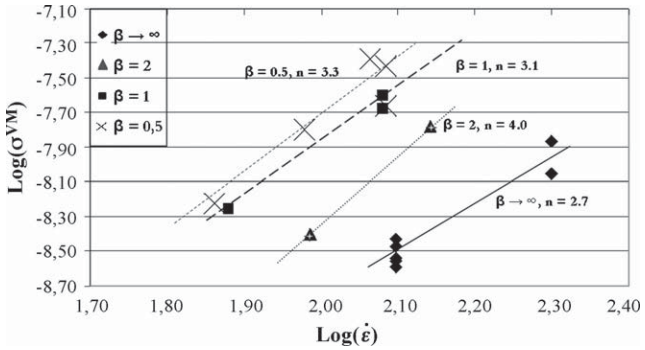

Fig. 6. Map of the deformations versus Von Mises Stress for each kind of creep tests.

4. Discussion and conclusion

The anisotropy of the Zircaloy 4 has been well highlighted, in terms of thermal but also mechanical behaviour. Moreover, the results obtained under multi-axial loadings in the present study are coherent with results already presented in the literature.

First of all, the present creep tests under internal pressure ($\beta = 0.5$) can be compared to Brenner's results [17]. Indeed for creep tests realised with hoop stresses of 113 MPa and 130 MPa, he observed r ratios, respectively, of 0.20 and 0.22. In the present study, we observed r ratios of 0.18 and 0.25 for a hoop stress of 140 MPa.

In the same way, the thermal expansion coefficients are comparable to those observed by Brachet et al. [18]. For a zirconium-based alloy ($Z > 98\%$), the dilatometric measurements realised between 473 K and 773 K ranged from $5.58 \times 10^{-6}\ K^{-1}$ to $8.31 \times 10^{-6}\ K^{-1}$, depending upon the cutting range of the sample, leading to a thermal anisotropy ratio of 0.67.

Lastly, the Norton coefficients observed are in good agreement with the coefficients n presented by Charit and Murty [19] for zirconium alloys, since for zirconium alloys of class A (Nb-Zr) and class M (Zircaloys) n is equal, respectively, to 3 and 4 for temperatures ranging from 623 K to 773 K. Nevertheless further tests are needed to confirm the dependence of n upon β.

This new device specially adapted to cladding tube testing allows us to lead a large range of creep tests, and thus to increase the present data base on zirconium alloys. As a consequence, with a better knowledge of the practical thermomechanical behaviour of these materials, we will be able to improve the polycrystalline models used to predict the mechanical behaviour of these alloys under various thermal creep conditions.

References

[1] K.L. Murty, B.L. Adams, Mater. Sci. Eng. 70 (1985) 169–180.
[2] V. Fidleris, J. Nucl. Mater. 26 (1968) 51–76.
[3] R.A. Holt, J. Nucl. Mater. 8 (1979) 419–429.
[4] Y.S. Kim, J. Nucl. Mater. 250 (1997) 164–170.
[5] E. Tenckhoff, Deformation Mechanisms, Texture, and Anisotropy in Zirconium and Zircaloy, ASTM Special Technical Publication, Philadelphia, USA, 1988.
[6] P. Delobelle, P. Robinet, P. Geyer, P. Bouffioux, J. Nucl. Mater. 238 (1996) 135–162.
[7] I. Schäffler, P. Geyer, P. Bouffioux, P. Delobelle, J. Eng. Mater. Technol. 122 (2000) 169–176.
[8] D. Kaddour, Fluage isotherme et anisotherme dans les domaines monophasés (alpha et béta) et biphasés (alpha + béta) d'un alliage Zr–1%NbO. Ph.D. Ecole Nationale des Mînes de Paris, France, 2004.
[9] J.J. Fundenberger, M.J. Philippe, F. Wagner, C. Esling, Acta Mater. 45 (1997) 4041–4055.
[10] C. Grosjean, D. Poquillon, J.-C. Salabura, J.-M. Cloué, in: A. Gupta (Ed.), Proceedings of the 19th International Conference on Structural Mechanics in Reactor Technology, Toronto, Canada, August 12–17, 2007.
[11] D. Kaddour, S. Fréchinet, A.F. Gourgues, J.-C. Brachet, L. Portier, A. Pineau, Scr. Mater. 51 (2004) 515–519.
[12] J.C. Earthman, K.L. Murty, B.V. Tanikella, J.C. Britt, JOM 46 (1994) 48–54.

[13] F. Ferrer, Etude des mécanismes de déformation du zirconium entre 25 °C et 400 °C. Influence d'une faible teneur en soufre. Ph.D. Ecole polytechnique, Paris, France, 2000.
[14] F. Onimus, Approche expérimentale et modélisation micromécanique du comportement des alliages de zirconium irradiés. Ph.D. Ecole centrale Paris, Paris, France, 2003.
[15] D. François, A. Pineau, A. Zaoui, Hermès, Hermès Editions, Comportement mécanique des matériaux, vol. 1, Paris, France, 1995.
[16] D. François, A. Pineau, A. Zaoui, Hermès, Hermès Editions, Comportement mécanique des matériaux, vol. 2, Paris, France, 1995.
[17] R. Brenner, Influence de la microstructure sur le comportement en fluage thermique d'alliages de zirconium: analyse expérimentale et mise en œuvre de méthodes d'homogénéisation. Ph.D. Université Paris XIII, France, 2001.
[18] J.C. Brachet, J.L. Béchade, A. Castaing, L. Le Blanc, T. Jouen, Mater. Sci. Forum 273–275 (1998) 529–534.
[19] I. Charit, K.L. Murty, in: A. Gupta (Ed.), Proceedings of the 19th International Conference on Structural Mechanics in Reactor Technology, Toronto, Canada, August 12–17, 2007.